Supporting Information

Solution Processed Infrared- and Thermo- Photovoltaics based on 0.7 eV Bandgap PbS Colloidal Quantum Dots

*Yu Bi[1], Arnau Bertran[1], Shuchi Gupta[1], Iñigo Ramiro[1], Santanu Pradhan[1], Sotirios Christodoulou [1], Shanmukh-Naidu Majji[1], Mehmet Zafer Akgul[1], and Gerasimos Konstantatos[1, 2]***

1. ICFO—Institut de Ciencies Fotoniques, The Barcelona Institute of Science and Technology, Av. Carl Friedrich Gauss, 3, 08860 Castelldefels (Barcelona), Spain
2. ICREA—Institució Catalana de Recerca i Estudis Avançats, Passeig Lluís Companys 23, 08010 Barcelona, Spain

***E-mail:** Gerasimos.Konstantatos@icfo.eu

Experimental Section

PbS CQDs synthesis: 1.3 eV PbS CQDs were synthesized with a standard reported recipe. [1]0.93 eV and 0.7 eV PbS CQDs were synthesized via our previous reported multi-injection methods with minor modifications.[2, 3] Typically, 0.45 g of PbO was dissolved in 50 ml of 1-octadecene (ODE) and 3.8 ml of oleic acid under vacuum at 95 °C. After 12 h, the temperature was adjusted to 100 °C. Different amounts of Hexamethyldisilathiane (TMS) were dissolved in ODE respectively. 4 injections were done to get the desired CQDs. For 0.93 eV PbS CQDs, 90 μl TMS for the first injection and 25 μl × 3 TMS for the additional 3 injections were needed. The solution of 90 μl TMS was injected into the lead precursor solution at 100 °C, the additional 3 injections were sequentially followed at regular intervals of 6 mins. When the injection finished, the flask was allowed to gradually cool down to room temperature under stirring. To get 0.7 eV PbS CQDs, all the reaction processes remain the same as the 0.93 eV PbS CQDs, except that the first injection solution was reduced to 60 μl TMS. CQDs were purified in air by adding acetone, followed by centrifugation. The final CQDs were dispersed in toluene with a concentration of 40 mg/mL for the solar cell fabrication.

Chlorine doped ZnO nanocrystal synthesis: ZnO nanocrystals were synthesized via a previous reported method.[4] Chlorine doped ZnO nanocrystals (Cl_ZnO) were prepared with the reported recipe.[5] 10 mg/mL NaCl in methanol was mixed with 40 mg/mL ZnO in chloroform. (Volume ratio of NaCl and ZnO is 1:4)

Device fabrication: ITO glass substrates were cleaned in ultrasonic bath by using the soap water, distilled water, acetone and isopropanol, respectively. As-prepared Cl_ZnO were spin-coated on the cleaned ITO glass substrate at 3500 rpm for 30 s. The Cl_ZnO film was annealed at 260 °C in ambient. The active layer was deposited by a layer-by-layer spin coating method. 0.7 eV PbS CQDs with concentration of 40 mg/mL covered the whole substrate, followed by spinning at 2500 rpm for 20 s. ZnI_2/MPA ($25X10^{-3}$ M with 0.01% MPA in methanol) solution covered the PbS layer for 10 s before spinning at 2500 rpm for 10 s. The spinning substrate was flushed twice by few drops of methanol and spun for 20 s to make film dry. The above process was repeated till the desired thickness was achieved. The electron blocking layer of the solar cells comprise two layers of 0.02% V/V EDT treated PbS CQDs. The PbS film was covered by EDT acetonitrile solution for 30 s before spun at 2500 rpm for 10 s. The spinning substrate was flushed by 10 drops of acetonitrile followed by spinning for 20 s to make film dry. The above process was repeated twice to obtain the electron blocking layer. All the PbS CQDs layer fabrication process was carried out in a fume hood in ambient. 80 nm Au was deposited on the films by thermal evaporation at a speed of 1 Å s^{-1} by using a Kurt J. Lesker Nano 36 system at a base pressure lower than 10^{-6} mbar. The solar cells were transferred from the evaporator into the glove box for annealing at 140 °C for 5 min. The active area of the device is 3.14 mm^2. All the devices were taken out of the glovebox and stored in air for the further characterization.

S1. Simulated EQE curves of PbS CQDs solar cell with transfer matrix method

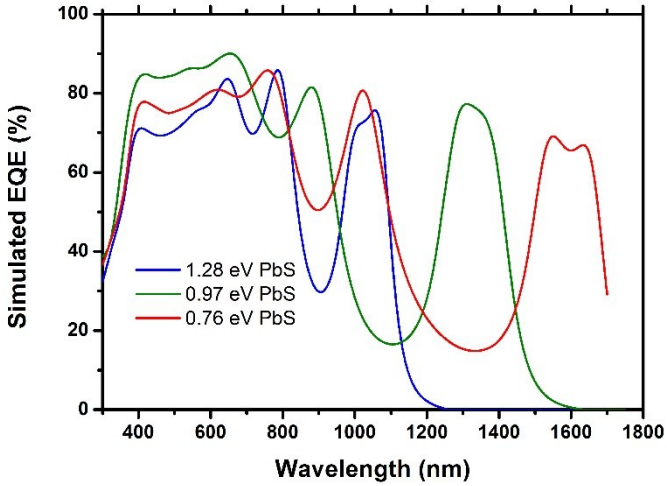

Figure S1. Simulated EQE curves with device structure ITO (80 nm)/ZnO(40 nm)/PbS/Au (80 nm). For PbS CQDs with varied band gap, the optimized active layer thickness changes according to the TMM simulation. For 1.28 eV, 0.97 eV and 0.76 eV PbS, active layer thickness is 470 nm, 400 nm and 470 nm, respectively.

S2. Optical property and TEM image of the as-obtained PbS CQDs.

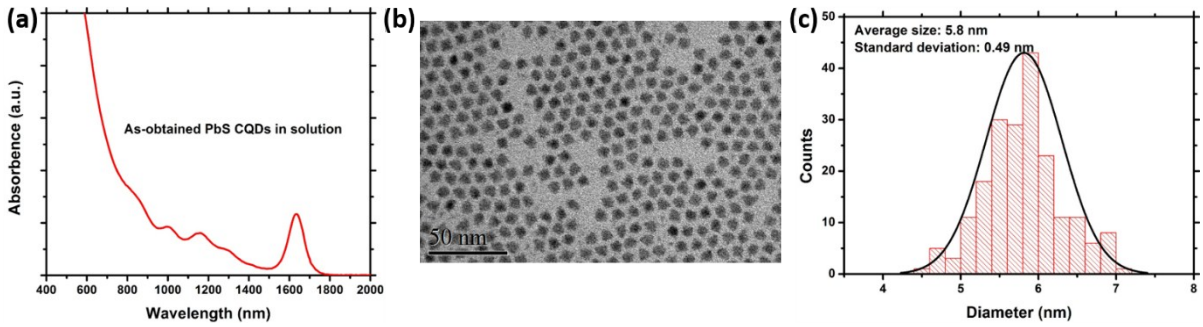

Figure S2. (a) Absorption spectrum of as-obtained PbS CQDs in toluene; (b) TEM image of the corresponding as-obtained PbS CQDs, and (c) Sizing histogram of the corresponding CQDs with the normal fitting. (The data were collected from 200 CQDs for the size distribution in TEM image by ImageJ software)

S3. The selection of electron blocking layer for 0.7 eV PbS CQD solar cells

EDT treated PbS CQDs layer has been used as a standard electron blocking layer ever since it was reported due to the more p-type inducing ligand EDT comparing to the halide ligands.[6-10] To engineer the band alignment between the active layer and Au electrode, PbS CQDs with varied band gaps offer us more choices to select the perfect candidate for the electron blocking layer. Here, 1.3 eV, 0.93 eV and 0.7 eV PbS CQDs were utilized as the electron blocking layer, respectively, for 0.7 eV PbS CQDs solar cell. Device performance is summarized in **Table S2**. With the 1.3 eV PbS CQDs as an electron blocking layer, device performance clearly stands out among others with better J_{SC}, V_{OC}, FF and PCE. Especially the substantially improvement in J_{SC} up to 33.15 mA/cm^2 from 28 mA/cm^2 have been achieved as we expected with better band alignment. EQE spectrum has been recorded in **Figure S3d**. The similar peak around 866 nm observed in all the devices stems from Fabry-Perot mode, suggesting the thicknesses of the devices are similar to each other, thus ruling out the possibility of varied J_{SC} due to the differences in device thickness.

UPS measurements have been carried out on ZnI_2/MPA treated PbS CQD film and EDT treated PbS films, detailed UPS spectra are present in **Figure S3a, b**. Energy level alignments are presented in **Figure S3c**, the relatively similar valence band gap between ZnI_2/MPA treated 0.7eV PbS CQD layer and the EDT treated PbS CQD layers indicate the similar hole transporting capability among these EDT treated PbS CQD layers. Yet, the huge difference among the conduction band gap between them suggests that EDT treated 1.3 eV PbS CQD layer outperforms others as the electron blocking layer.

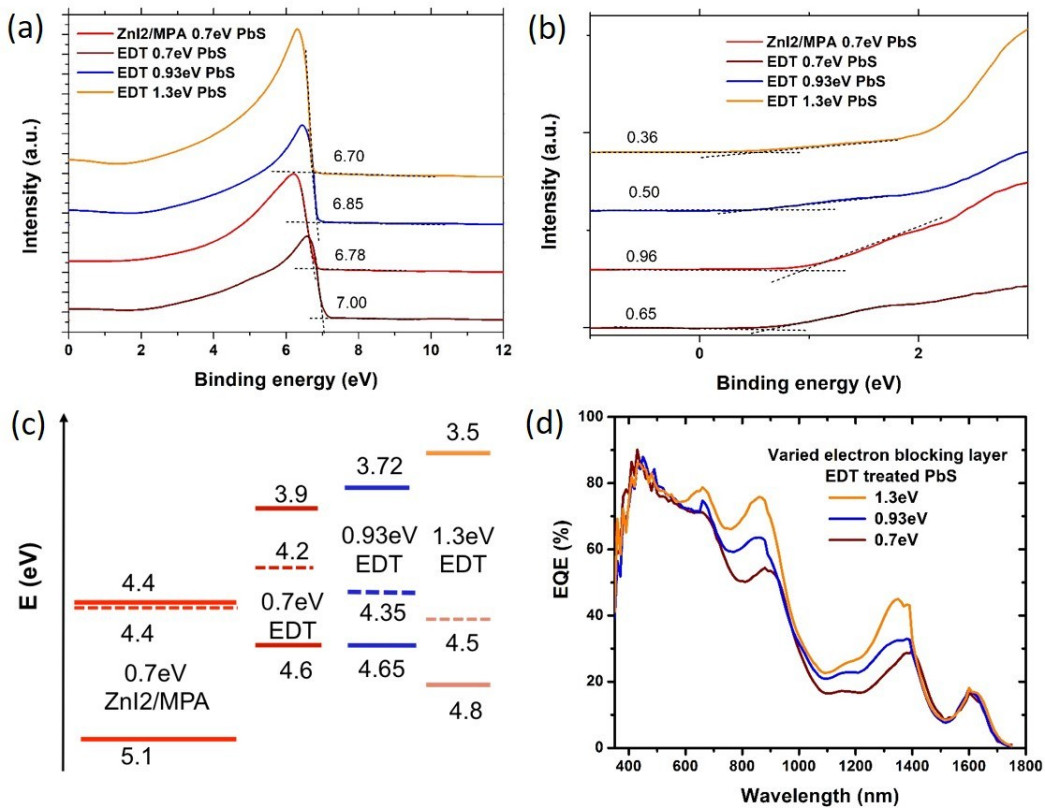

Figure S3. UPS spectra of PbS CQDs with varied bandgap and different ligand treatments deposited on top of ITO substrates, (a) work function region and (b) valence band region. (c). The energy level diagram of the PbS components referenced to the vacuum level based on the data shown in (Figure S3a, b) and (d) Measured EQE curves of the solar cells with varied electron blocking layers.

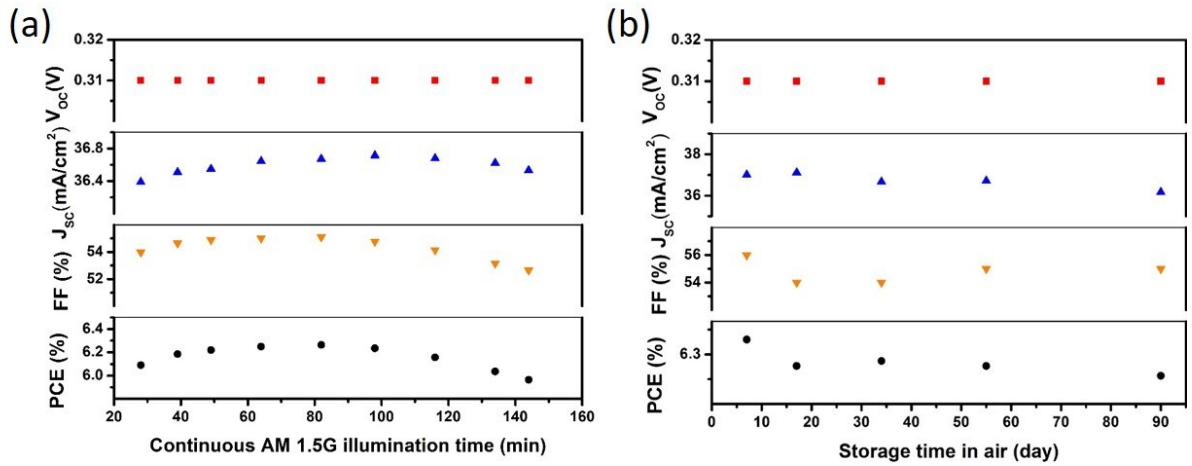

Figure S4. (a) Photostability measurements under continuous AM 1.5G simulated solar illumination in air with non-encapsulated device, (b) Long term stability test of a non-encapsulated device stored in ambient air conditions.

Tables:

Table S1 Effect of electron acceptors on the device performance.

Varied electron acceptors	V_{OC} [V]	J_{SC} [mA/cm^2]	FF [%]	PCE [%]	R_S [Ω]	R_{SH} [KΩ]
Cl_ZnO	0.35	31.56	54	6.0	24	2.79
ZnO	0.33	26.50	55	4.8	31	3.09

Table S2. Device performance summary on varied blocking layers.

Varied blocking PbS layer	V_{OC} [V]	J_{SC} [mA/cm^2]	FF [%]	PCE [%]	R_S [Ω]	R_{SH} [KΩ]
Ref. (0.7 eV)	0.32	28.45	57	5.16	19	2.34
1.3 eV	0.34	33.15	56	6.33	35	3.27
0.93 eV	0.33	31.00	54	5.54	20	2.15

Table S3 Variation of the active layer thickness effect on the device performance

Thickness variation of the PbS CQDs layer	V_{OC} [V]	J_{SC} [mA/cm^2]	FF [%]	PCE [%]	R_S [Ω]	R_{SH} [KΩ]
385nm	0.29	36.60	52	5.49	21	3.54
435nm	0.31	37.01	56	6.39	22	4.70
485nm	0.3	34.24	55	5.67	20	3.75

References:

1. S. Pradhan, A. Stavrinadis, S. Gupta, Y. Bi, F. Di Stasio and G. Konstantatos, *Small*, 2017, **13**.
2. B. Yu, P. Santanu, G. Shuchi, A. M. Zafer, S. Alexandros and K. Gerasimos, *Adv Mater*, 2018, **30**, 1704928.
3. S. Goossens, G. Navickaite, C. Monasterio, S. Gupta, J. J. Piqueras, R. Pérez, G. Burwell, I. Nikitskiy, T. Lasanta, T. Galán, E. Puma, A. Centeno, A. Pesquera, A. Zurutuza, G. Konstantatos and F. Koppens, *Nat Photon*, 2017, **11**, 366.
4. Y. Cao, A. Stavrinadis, T. Lasanta, D. So and G. Konstantatos, *Nat. Energy*, 2016, **1**, 16035.
5. J. Choi, Y. Kim, J. W. Jo, J. Kim, B. Sun, G. Walters, F. P. Garcia de Arquer, R. Quintero-Bermudez, Y. Li, C. S. Tan, L. N. Quan, A. P. T. Kam, S. Hoogland, Z. Lu, O. Voznyy and E. H. Sargent, *Adv Mater*, 2017, **29**, 1702350.
6. C.-H. M. Chuang, P. R. Brown, V. Bulović and M. G. Bawendi, *Nat Mater*, 2014, **13**, 796-801.
7. J. Xu, O. Voznyy, M. Liu, A. R. Kirmani, G. Walters, R. Munir, M. Abdelsamie, A. H. Proppe, A. Sarkar, F. P. García de Arquer, M. Wei, B. Sun, M. Liu, O. Ouellette, R. Quintero-Bermudez, J. Li, J. Fan, L. Quan, P. Todorovic, H. Tan, S. Hoogland, S. O. Kelley, M. Stefik, A. Amassian and E. H. Sargent, *Nat Nanotech*, 2018, **13**, 456-462.
8. M. Liu, O. Voznyy, R. Sabatini, F. P. Garcia de Arquer, R. Munir, A. H. Balawi, X. Lan, F. Fan, G. Walters, A. R. Kirmani, S. Hoogland, F. Laquai, A. Amassian and E. H. Sargent, *Nat Mater*, 2017, **16**, 258-263.
9. X. Lan, O. Voznyy, F. P. Garcia de Arquer, M. Liu, J. Xu, A. H. Proppe, G. Walters, F. Fan, H. Tan, M. Liu, Z. Yang, S. Hoogland and E. H. Sargent, *Nano Lett*, 2016, **16**, 4630-4634.
10. A. H. Ip, A. Kiani, I. J. Kramer, O. Voznyy, H. F. Movahed, L. Levina, M. M. Adachi, S. Hoogland and E. H. Sargent, *ACS Nano*, 2015, **9**, 8833-8842.